Stratospheric profiles of nitrogen dioxide observed by Optical Spectrograph and Infrared Imager System on the Odin satellite

Christopher E. Sioris,[1] Craig S. Haley,[2] Chris A. McLinden,[3] Christian von Savigny,[4] Ian C. McDade,[2] Jack C. McConnell,[2] Wayne F. J. Evans,[5] Nicholas D. Lloyd,[6] Edward J. Llewellyn,[6] Kelly V. Chance,[1] Thomas P. Kurosu,[1] Donal Murtagh,[7] Urban Frisk,[8] Klaus Pfeilsticker,[9] Hartmut Bösch,[9] Frank Weidner,[9] Kimberly Strong,[10] Jacek Stegman,[11] and Gérard Mégie[12]

Received 19 June 2002; revised 5 November 2002; accepted 19 December 2002; published 9 April 2003.

[1] Vertical profiles of nitrogen dioxide in the 19–40 km altitude range are successfully retrieved over the globe from Optical Spectrograph and Infrared Imager System (OSIRIS) limb scatter observations in late 2001 and early 2002. The inclusion of multiple scattering in the radiative transfer model used in the inversion algorithm allows for the retrieval of NO_2 down to 19 km. The slant column densities, which represent the observations in the inversion, are obtained by fitting the fine structure in normalized radiance spectra over the 435–449 nm range, where NO_2 electronic absorption is readily observable because of long light paths through stratospheric layers rich in this constituent. Details of the spectral fitting and inversion algorithm are discussed, including the discovery of a pseudo-absorber associated with pixelated detectors and a new method to verify altitude registration. Comparisons are made with spatially and temporally coincident profile measurements of this photochemically active trace gas. Better than 20% agreement is obtained with all correlative measurements over the common retrieval altitude range, confirming the validity of OSIRIS NO_2 profiles. Systematic biases in the number densities are not observed at any altitude. A "snapshot" meridional cross section between 40°N and 70°S is shown from observations during a fraction of an orbit. *INDEX TERMS:* 0340 Atmospheric Composition and Structure: Middle atmosphere—composition and chemistry; 0360 Atmospheric Composition and Structure: Transmission and scattering of radiation; 0394 Atmospheric Composition and Structure: Instruments and techniques; 3334 Meteorology and Atmospheric Dynamics: Middle atmosphere dynamics (0341, 0342); *KEYWORDS:* optical, Sun-synchronous, polar-orbiting, Fraunhofer, Ring effect, iterative onion peel

Citation: Sioris, C. E., et al., Stratospheric profiles of nitrogen dioxide observed by Optical Spectrograph and Infrared Imager System on the Odin satellite, *J. Geophys. Res.*, *108*(D7), 4215, doi:10.1029/2002JD002672, 2003.

1. Introduction

[2] *Crutzen* [1970] first discussed the importance of catalytic destruction of ozone by NO_x ($NO + NO_2$). Reactions involving NO_x dominate stratospheric ozone loss between 24 and ~45 km [*Garcia and Solomon*, 1994; *Crutzen*, 1971]. NO_x measurements in the lower stratosphere are also important because of the coupling with ClO_x and HO_x cycles. The loss of NO_2 through its conversion to HNO_3 can be used as a diagnostic of ozone hole heterogeneous chemistry. OSIRIS (Optical Spectrograph and Infrared Imager System) is capable of measuring not only profiles of stratospheric ozone [*von Savigny et al.*, 2003] but, as will be demonstrated here, the vertical

[1]Atomic and Molecular Physics Division, Harvard-Smithsonian Center for Astrophysics, Cambridge, Massachusetts, USA.
[2]Centre for Earth and Space Science, York University, Toronto, Ontario, Canada.
[3]Meteorological Service of Canada, Environment Canada, Toronto, Ontario, Canada.
[4]Institute of Environmental Physics, University of Bremen, Bremen, Germany.
[5]Department of Physics, Trent University, Peterborough, Ontario, Canada.
[6]Department of Physics and Engineering Physics, University of Saskatchewan, Saskatoon, Saskatchewan, Canada.
[7]Department of Radio and Space Science, Chalmers University, Göteberg, Sweden.
[8]Swedish Space Corporation, Solna, Sweden.
[9]Institute of Environmental Physics, University of Heidelberg, Heidelberg, Germany.
[10]Department of Physics, University of Toronto, Toronto, Ontario, Canada.
[11]Department of Meteorology, Stockholm University, Stockholm, Sweden.
[12]Service d'Aeronomie, Centre National de la Recherche Scientifique, Institut Pierre-Simon Laplace–Université Pierre et Marie Curie, Paris, France.

0148-0227/03/2002JD002672$09.00

distribution of nitrogen dioxide (NO_2) as well. It is one of two limb-viewing instruments onboard the Swedish Sun-synchronous satellite Odin. The other instrument is a sub-mm radiometer (SMR), which also observes the stratospheric limb.

[3] Odin is a small, low cost satellite that will split its expected lifetime of two years alternating between aeronomic and astronomic observation on a daily basis [*Murtagh et al.*, 2002]. As of February 20th of 2001, Odin ascends over the equator toward the North Pole at 6 pm local time in a near-terminator orbit at an inclination of 97.8°, providing 15 orbits/day. Its orbit is such that OSIRIS cannot make dayside measurements in the winter hemisphere near solstice. In terms of aeronomy, the main mission of Odin is to monitor the stratospheric ozone layer. This is achieved by spectral measurements of UV and visible limb radiance. The Odin satellite scans the limb at a rate of approximately 0.75 km/s and OSIRIS, which looks in the forward along-track direction, collects a spectral image every ~2 km in tangent height (TH). Scans usually cover the range from $7 \leq TH \leq 70$ km when Odin is in stratospheric mode and up to TH = 100 km in stratospheric-mesospheric (strat/meso) mode. One scan of the limb in stratospheric mode takes ~1.5 minutes, so the spacecraft will have covered ~600 km in the along-track direction (or ~5° in latitude).

[4] Thus far, the limb scatter technique from above the atmosphere has only been applied to the retrieval of two stratospheric gases: ozone (e.g., by SOLSE/LORE [*Flittner et al.*, 2000]) and NO_2 by the Solar Mesosphere Explorer (SME, [e.g., *Thomas et al.*, 1988, and references therein]). The SME was a two channel visible spectrometer with a 3.5 km field of view (FOV) that could only observe one NO_2 differential feature at a time. POAM (Polar Ozone and Aerosol Measurement) III and SAGE II also measure NO_2 profiles but only at twilight and thus have limited spatial and temporal coverage. Similarly to SME, both instruments use only one wavelength pair corresponding to one NO_2 spectral feature: 448 and 453 nm for SAGE II [*Cunnold et al.*, 1991], 439.6 and 442.2 nm for POAM III [*Lucke et al.*, 1999]. In contrast, the retrieval algorithm briefly described here uses 37 of the 1353 pixels in the part of the spectral range of OSIRIS where four of the most identifiable NO_2 vibronic absorption structures appear. Thus, for the above reasons, the NO_2 profiles retrieved from OSIRIS limb spectra rely on an improved technique in satellite remote sensing. The use of many wavelengths as compared to only an "on" and "off" wavelength pair allows for much better discrimination between optical depth due to NO_2 and that caused by ozone and scattering [*McElroy*, 1988].

[5] In this paper, we show an initial validation of NO_2 profile measurements for different times of day, year and for a variety of latitudes. Good limb scanning was first achieved in late June 2001. Fairly consistent limb scanning began in late July. Profile measurements presented here will come from August, October, and February data in particular. Sample profiles are validated with profiles from three other coincident instruments that possess equal or better vertical resolution than OSIRIS. This provides insight into the ability of OSIRIS and the inversion algorithm to retrieve the shape and magnitude of the number density profile. Validated global 3-D maps of NO_2 will be presented in future work.

2. Method

[6] A detailed description of the OSIRIS instrument is available elsewhere [*Warshaw et al.*, 1996; *Llewellyn et al.*, 1997]. Here we will highlight the important instrumental characteristics. OSIRIS has an instantaneous field of view (IFOV) of ~1 km in the vertical and 40 km in the across-track horizontal direction with the slit of the spectrograph being oriented parallel to the limb. Although spectral images of the limb are recorded presently every ~2 km in tangent height (TH), the vertical sampling can be improved at the expense of a lower signal to noise (S/N) ratio with simple software changes to the auto-exposure algorithm. Across-track horizontal inhomogeneities can be resolved as the 40 km swath is provided by 32 pixel rows in the spatial dimension of the 2-D charge-coupled device (CCD). These 32 rows are binned together by default to reduce the data flow and improve S/N. Thus, ~1 km horizontal sampling is achievable when OSIRIS images in the across-track dimension. The IFOV of OSIRIS compares favourably with that of the recently launched SCIAMACHY in limb viewing mode [*Bovensmann et al.*, 1999]. In the spectral dimension, OSIRIS measures electromagnetic radiation in the 280–800 nm range with ~1 nm spectral resolution (full-width at half-maximum) and each of its 1353 CCD detector pixels cover ~0.4 nm in the spectral domain, leading to a fairly well sampled spectrum.

[7] The retrieval of NO_2 profiles is considerably simplified by separating it into two smaller problems [*McDade et al.*, 2002]. The first step is to determine the observed slant column densities (SCDs) of NO_2 by linear least squares fitting of the observed differential spectral structure. The second step is the inversion of the slant column density profiles to obtain local number density profiles. A global fitting approach [*Carlotti*, 1988] where all spectra and all tangent heights in a limb scan are fit by varying concentrations of a number of different absorbing constituents at a number of different heights was judged to be too computationally expensive and more complicated with regards to troubleshooting.

2.1. Spectral Fitting

2.1.1. Fraunhofer Reference

[8] The differential optical absorption spectroscopy (DOAS) technique [*Noxon*, 1975] is used for the spectral fitting with some modifications. High TH spectra ($50 < TH < 70$ km, even in strat/meso mode) from the same limb scan are co-added and used as a Fraunhofer reference spectrum (I_0) as they contain only weak NO_2 absorption from multiply scattered contributions to the source function. The near-terminator orbit leads to high solar zenith angles (SZA > 57°), thereby significantly reducing the impact of clouds and surface reflection. The normalization with lower mesospheric spectra from the same limb scan further reduces the importance of any underlying tropospheric signature as it cancels out to a first approximation in the ratio because the multiple-scattering contribution is only weakly altitude-dependent above 20 km [*Sioris*, 2001]. This point will be readdressed below.

2.1.2. Spectral Fitting Window

[9] The fitting window is chosen to be 434.7–449.0 nm because the largest differential NO_2 absorption structures lie therein. Differential optical depths (DODs) are as large as 2% at the peak of the slant column density profile. The fitting window must be kept small enough that the extinction over the fitting window is roughly constant otherwise the SCD is wavelength (λ) dependent. However, the window must contain enough pixels that none of the absorbers (or pseudo-absorbers) are strongly correlated and S/N is improved. The chosen window also avoids major Fraunhofer lines at ~431 and 434 nm. Large solar absorption features do not cancel completely regardless of which reference is used.

2.1.3. Ring Effect

[10] One reason for the imperfect cancellation is that a lower mesospheric reference is expected to have a different Ring effect signature [*Grainger and Ring*, 1962] than stratospheric limb spectra since temperature, aerosols, and multiple scattering are a function of altitude [*Sioris*, 2001] (available from www.geocities.com/csioris/thesis3.zip). The impact of residual Ring structures due to the altitude dependence of multiple scattering and filling in of NO_2 lines is quite small (leads to residuals on the order of 6×10^{-4} or less) in the 353–387 nm OClO fitting window for OSIRIS as shown using radiative transfer model (RTM) simulations [*Sioris*, 2001]. The temperature dependence of the rotational Raman scattering (RRS) cross sections can produce residual structures one order of magnitude larger ($\sim 10^{-3}$) and is much more important for limb viewing than in other geometries where the Ring effect has been observed (i.e., satellite-nadir [*Joiner et al.*, 1995], ground-based [*Sioris et al.*, 2002]) because radiance contribution functions peak more sharply at a certain altitude (or temperature) for limb viewing, usually at the tangent height. The residual does not match the filling-in spectral structure itself and is largest when the difference in effective temperature between the reference TH and the TH of interest is a maximum. The dilution of the inelastic signature of molecular scattering by elastic scattering from aerosols can be the most important of these altitude-dependent effects, particularly at longer wavelengths [*Sioris*, 2001].

[11] Before the observed spectral structure is fitted with the various absorbers and pseudo-absorbers, the Ring effect is removed from limb spectra in the 15 < TH (km) < 70 range with a single iteration of the backward Ring model [*Sioris et al.*, 2002]. To correct the radiance spectrum (I) at a given tangent height, the temperature at the tangent height is assumed to be the effective temperature for the calculation of the RRS cross sections. The temperature profile is currently obtained as a function of latitude, longitude and time from the MSIS-E-90 model [*Hedin*, 1991] and only needs to be moderately accurate (i.e., ~8 K [*Sioris*, 2001]). The current implementation of the backward model assumes a purely molecular scattering atmosphere, although in the case of a significant injection of particulate matter into the stratosphere an iterative version of the model [*Sioris*, 2001] would be implemented.

2.1.4. Spectral Radiance Calibration

[12] Only one other step was required before beginning the spectral fitting. This involved recalibrating OSIRIS wavelengths by cross-correlation of a single normalized limb radiance spectrum from early in the mission (July 30th, 2001) with the NO_2 cross section [*Vandaele et al.*, 1998] convolved to OSIRIS resolution. No shifting or stretching has been applied subsequently and does not appear to be required based on analysis of spectral fits. This is consistent with the fact that the detector temperature has remained cool and steady throughout the period analyzed here. During an individual scan such as the down-scan containing the aforementioned spectrum, the detector temperature was -18.21 ± 0.05 °C. This suggests that wavelength stability should be very good over one limb scan and dark current should be minimal. Internal scattering, defined elsewhere [*Sioris et al.*, 2002], is extremely small (γ = 2e-6) based on analysis of in-flight radiance profiles at short wavelengths (<305 nm) and low TH where little signal is expected. This value of γ is slightly lower than the value measured in laboratory tests on the flight model [*Evans and Alfred*, 2001]. Thus, in the 435–450 nm interval, internal scattering is trivial relative to the signal. Wood's anomalies are another cause of artificial spectral structure. The closure polynomial adequately removes any instrumental sensitivity to the Q (and U) Stokes component of the polarization as fortunately OSIRIS has no Wood's anomalies in this spectral interval [*McLinden et al.*, 2002]. Also, baffle scattering does not appear to be a significant issue in the blue for TH < 70 km. This was confirmed by examining the linearity of a plot of ln(radiance) vs. TH above the stratospheric aerosol layer.

2.1.5. Absorbers

[13] For stratospheric tangent heights, the differential absorption in this fitting window is almost entirely caused by absorption by NO_2 and O_3. A known atmospheric feature due to water vapour at ~442.6 nm regularly observed from nadir and zenith-viewing geometry [e.g., *Johnston and MacKenzie*, 1989] has not appeared in the normalized limb radiance spectra. Water vapour reference spectra [*Camy-Peyret et al.*, 1985; *Zobov et al.*, 2000] have not helped fits. We have also not been able to match the absorption feature of the O_2-O_2 collisional complex at 446.7 nm [*Greenblatt et al.*, 1990] although this is not surprising considering that for similar observing geometry and path lengths, *Pfeilsticker et al.* [2001] only retrieved the vertical profile of the O_2-O_2 collisional complex up to 14 km. Thus, these are expected to be interfering species at lower tangent heights. The absolute absorption cross section of NO_2 at 220 K of *Vandaele et al.* [1998] is chosen because it is the current HITRAN standard and is accurate to <3%. Also, SCIAMACHY laboratory reference data at 203, 223, and 243 K [*Bogumil et al.*, 1999] are used because of the number of available temperatures and the known, albeit weak temperature dependence of NO_2 absorption in this spectral range [e.g., *Vandaele et al.*, 1998]. For ozone, the cross section of *Burrows et al.* [1999a] at 202 K was chosen although in the fitting window, the ozone differential absorption is spectrally smooth and/or weak enough that the SCD profile of this interfering trace gas cannot be recovered reliably and is correlated with the closure polynomial. These absorption cross sections are convolved and binned to instrumental parameters of the optical spectrograph (OS). The convolution takes into account the spectral resolution of the source instrument (e.g., SCIAMACHY) by assuming that all

instrument functions are well approximated by a gaussian line shape.

2.1.6. Differential Cross Sections

[14] The differential cross sections are obtained by fitting a low order polynomial to each of the absolute cross sections over a larger spectral range than the fitting window to ensure that the spectrally smooth component of the absorption is removed without fitting any of the fine structure with the polynomial. Polynomials are in terms of pixel number (n) starting with 1 at the blue end of the differential window and the increment is 1 per pixel. This allows a low order polynomial to be more flexible than a polynomial in wavelength. The difference between using differential and absolute cross sections was found to be trivial in this fitting window, as the polynomial closure term in equation (1) appears to compensate for the spectrally smooth component of the NO_2 and ozone absorption.

2.1.7. Temperature Dependence

[15] Intermediate temperatures (e.g., T = 216 K) are obtained by linear interpolation between differential forms of the *Bogumil et al.* [1999] set of NO_2 cross sections. The ensemble of different temperatures (e.g., 203, 216, 220, 223, 243) are tried sequentially (not simultaneously) with each normalized radiance spectrum and the SCD for that observation is the SCD obtained with the NO_2 cross section giving the smallest fitting residual. Differential cross sections linearly interpolated to an intermediate temperature (i.e., 216 K) did not work well. In general, the most effective cross section is that of *Vandaele et al.* [1998] at 220 K followed by that of Bogumil et al. at 203 K. It appears that the temperature dependence of NO_2 is secondary in importance to the quality of the reference spectra. The best method to handle this temperature dependence is still under investigation.

2.1.8. Fitting Equation

[16] The linear regression model is

$$\ln(I_0/I) = SCD_{NO_2} d\sigma_{NO_2}(T) + SCD_{O_3} d\sigma_{O_3}(T) + c_{tilt} dtilt + A\,n^2 + B\,n + C, \quad (1)$$

where I is the radiance spectrum at the tangent height of interest, $d\sigma$ are the differential absorber cross sections, and c_{tilt} is the fitting coefficient for the tilt differential pseudo-absorber cross section (dtilt) described below. At high optical depths, the normalized radiance is highly sloped (i.e., wavelength trended) even over a narrow fitting window and up to a 4th order polynomial may be required. The optimal handling of the closure polynomial remains under investigation. The direct fitting method [*Chance*, 1998], in which $-\ln(I_0)$ is used as a basis function in fitting $-\ln I$, gives slightly larger uncertainties and residuals than simultaneous fitting of $\ln(I_0/I)$ for the cases we have attempted. We are unsure of the reason for this and further testing is required.

2.1.9. Tilt

[17] Fraunhofer structure does not cancel out in the normalization for a second reason, which to our knowledge, has not been discussed previously. It results partly from spectral undersampling. A sampling ratio of $\geq$4.5 pixels/FWHM is typically required in fitting NO_2 [*Roscoe et al.*, 1996]. This is almost twice the sampling ratio of OSIRIS and more than twice the sampling ratio of GOME in this window [*Burrows et al.*, 1999a]. It was noticed that, in OSIRIS limb radiance profiles, the pixel with the local minimum in radiance corresponding to a Fraunhofer line centre is a function of tangent height. The effect is partially attributable to the physical discretization of the spectral radiance by pixelated detectors and also due to the differently sloped continua of I and I_0. Spectral fine structure is introduced in the wings of Fraunhofer lines when the spectrum of interest and the spectrum used for normalization (i.e., TH = 70 km) do not have the same slope. The largest spectral structure is introduced when the core of a Fraunhofer line lies near the boundary between two adjacent pixels and is further compounded by instruments with "dead space" between pixels. The differences in slope are due to atmospheric processes; Rayleigh extinction, and Mie scattering are functions of altitude and either process can explain this effect. The difference in slope results in a different partitioning of the Fraunhofer line in the adjacent pixels. Because of the strong wavelength dependence of Rayleigh scattering, this phenomenon is most pronounced in the blue and UV and is aggravated by the long paths provided by limb viewing geometry. Hγ is an example of a Fraunhofer line for which the pixel with the minimum radiance actually depends on TH. The difference in superimposed NO_2 absorption between the pixels is not significant to the apparent line depth of Hγ. RRS also cannot cause this effect because the filling in is quite symmetrical about the line centre, especially for narrow (<0.9 nm) lines [*Sioris et al.*, 2002]. At low tangent heights, the pixel with the minimum radiance at Hγ shifts to the blue by one pixel due to Rayleigh extinction.

[18] To remove this atmospheric/instrumental spectral artefact we have dubbed 'tilt', we have used a combination of atmospheric and instrumental radiative transfer modelling to generate a pseudo-absorber spectrum to be used in the NO_2 fitting. Using MODTRAN4 [*Berk et al.*, 1999], the first step involved calculating highly resolved and sampled (1 cm^{-1}) spectral radiances at a low and high TH (16 and 70 km, respectively) for a non-absorbing atmosphere. We then convolved both these spectra and binned them according to the OSIRIS pixel-to-wavelength mapping and spectral resolution. After taking the ratio of the two spectra, and removing trending in the ratio with a quadratic, the fine structure introduced by this phenomenon was revealed (Figure 1). This pseudo-absorber has reduced fit residuals by a factor of two. In general, it appears to be important when: (1) spectral fitting windows include strong Fraunhofer lines; (2) the slope of the reference spectrum and spectrum of interest are not identical; and (3) detectors have pixels with intermediate spectral widths. When pixels or bandpasses are much wider than the apparent Fraunhofer line width, Fraunhofer structure becomes less important, e.g., NO_2 channels of POAM III. When pixels are much narrower than a strong Fraunhofer line, there are a sufficient number of bins over its width leading an adequate representation of its shape. This is the case for GOME channel 2 where a pixel is 0.11 nm wide and the equivalent width of the Fe I line at 358 nm is 0.21 nm [*Moore et al.*, 1966] even prior to convolution with the 0.17 nm FWHM instrument function of GOME [*Burrows et al.*, 1999b].

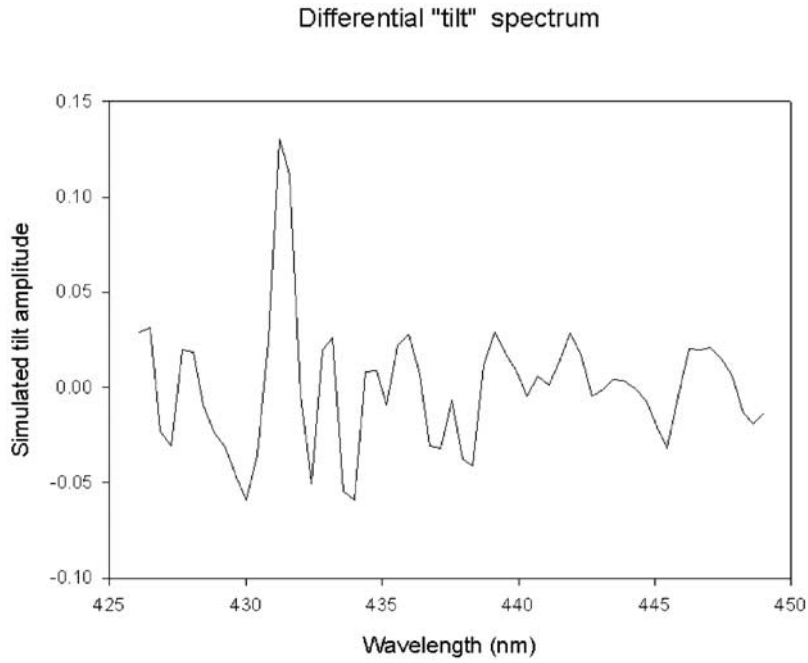

Figure 1. Simulated differential 'tilt' spectrum, appropriate for OSIRIS spectral resolution and binning in the 426–449 nm interval (see text for details).

[19] Based on simulations for the GOME BrO fitting window [*Chance*, 1998] with a solar reference and nadir radiance spectrum, we have calculated the importance of the pseudo-absorber and it is negligible (rms DOD of 7.7e-5) due partly to the narrower spectral binning of this instrument, whereas for OSIRIS, in the same fitting window, the 'tilt' rms DOD is 3.5e-4. In the NO_2 window, the 'tilt' rms DOD of OSIRIS is 1.0e-4. It is quite surprising that this effect was not discovered previously from observations made with detector pixels of intermediate spectral width, although an undersampling pseudo-absorber [e.g., *Chance*, 1998] or a shift and/or stretch algorithm [e.g., *Platt et al.*, 1997; *Sioris et al.*, 2002] could be partially compensating for the structure without including the essential physics of the phenomenon, as could smoothing of differential spectral structure. Fortunately NO_2, O_3 and 'tilt' are not strongly correlated with each other for OSIRIS in this fitting window so the inclusion of the tilt reference spectrum reduces the uncertainty of the retrieved NO_2 SCD but has no impact on the SCD itself.

2.2. Vertical Fitting: Inversion Algorithm

[20] After the SCDs of NO_2 are obtained as a function of tangent height, they are inverted to a yield a number density profile using a novel, iterative onion peeling (IOP) approach.

[21] The inversion consists of simulating SCDs in 2 km increments in TH and iteratively adjusting the number density profile until the simulated and measured SCDs converge at all tangent heights (18–40 km). In terms of vertically fitting the observed SCD profile with a simulated one, the method resembles the iterative least-squares inversion of *McDade et al.* [2002].

[22] The number densities are adjusted on the same 2 km grid. The grid is chosen to be comparable to the expected vertical resolution determined from averaging kernel calculations [*Strong et al.*, 2002]. A finer grid for the retrieval results in a zigzagging profile because the problem becomes underdetermined. The measured SCDs are interpolated onto the same grid using linear interpolation between the nearest two sampled THs or when vertical sampling is poor (ΔTH > 4.0 km), a 6th order polynomial fit (with typical $r^2 > 0.99$) to SCDs at THs sampled between 18–40 km is used. Interpolating the measured radiances onto the standard grid rather than the SCDs obscures the impact of satellite jitter in the retrieved SCD profile. Jitter during a down-scan affects S/N as the auto-exposure algorithm sets an exposure time appropriate for a lower (i.e., brighter) TH. The SCD uncertainties or χ^2 values from the linear least-squares fit can be used to determine which images were affected by jitter. These are omitted from the sextic fit to the SCD profile. Linear interpolation of SCDs is insufficient when the vertical sampling is poor (i.e., 4 km) due to irregular scanning (jitter) and results in an artefact in the retrieved number density at the height of the interpolation (and poor sampling).

[23] The OSIRIS tangent heights that are provided by the attitude control system (ACS) of Odin are verified independently (and occasionally corrected) using the 305 nm limb radiance profile. The quoted accuracy of the THs from the Odin ACS is <1.5 km. The tangent altitude of the 305 nm limb radiance maximum or 'knee' [*McPeters et al.*, 2000] is known from radiative transfer modeling and is insensitive to tropospheric clouds, surface albedo, and stratospheric aerosol because the upwelling radiation from the troposphere and lower stratosphere has been absorbed by stratospheric ozone. Using sensitivity studies, we have established that the knee is also very insensitive to temperature-related changes in number density and ozone absorption due to the weak temperature dependence at 305 nm. O_3

absorption is the main cause of the 305 nm knee. At 45 km, the overlying ozone column is largely governed by photochemistry, except at high latitudes [*Hilsenrath*, 1980], making it quite predictable. Observations over several orbits with OSIRIS and model calculations show the knee at 305 nm is at ~45 km. The insensitivity of the knee to these spatially variable geophysical parameters implies that the instrument measuring the limb radiance profile need not be a vertical imager for this technique to be applicable. Although the 305 nm knee exhibits some sensitivity to SZA, pressure, and mesospheric ozone, it is predictable using appropriate model atmospheres and scattering geometry. The precision of this technique is drastically improved by using spectral sampling to overcome Odin's vertical undersampling. A randomly chosen example from June 19th, 2001, at lat = 82°, and SZA = 59° will be presented to illustrate this technique. The first step is to find a set of pixel wavelengths that share the same knee TH using radiances on the measured TH grid such that the median wavelength is <305 nm. For this limb scan, there are exactly 6 pixel wavelengths ranging from 303.72–305.67 nm for which the knee is at TH = 45.589 km. For $\lambda < 303.7$ nm, the respective 'knees' are at higher THs and for $\lambda > 305.7$ nm, the 'knees' are at lower THs. The median wavelength of those six is 304.70 nm. Using vertically well-sampled simulations at 304.70 nm with MODTRAN4 for high-latitude summer and the appropriate geometry gives 45.6 km, indicating a difference between OSIRIS and MODTRAN4 of −11 m. After repeating this exercise at mid-latitudes over several orbits of data, the difference between the simulated and measured knee has a mean and standard deviation of 550 and 480 m, respectively. The non-zero mean is expected because the THs provided by the ACS do not include an accurate adjustment for the difference between the OSIRIS viewing angle and the Odin control frame. At high latitudes, it appears that due to its variability on timescales shorter than seasonal, the mesospheric O_3 column must be retrieved before or simultaneously with TH. Assuming accurate knowledge of pressure and mesospheric O_3, the overall accuracy of the technique approaches the limit imposed by the finite spectral sampling and resolution of OSIRIS and is <220 m.

[24] MODTRAN4 is the forward RTM used to simulate limb radiances in the $40 \geq$ TH (km) ≥ 16 range over the 22700–23000 cm^{-1} (434.8–440.5 nm) range at 20 cm^{-1} sampling and 45 cm^{-1} resolution (both appropriate for OSIRIS in this window). These spectra are then normalized with a simulated reference spectrum at the median TH used in the co-added observed reference spectrum (nominally TH = 60 km). MODTRAN4 includes refraction, and azimuthally varying higher order scattering [*Berk et al.*, 1999]. The solar geometry near the tangent point is used for the plane-parallel multiple-scattering calculation. The solar illumination on each layer is determined with spherical geometry. The DISORT 4-stream approximation is used thereby reducing the computational time significantly. The sensitivity of this assumption is quantified below (section 2.3). Then the simulated normalized spectra are fitted analogously to the measured normalized spectra using differential versions of the absolute cross sections of O_3 and NO_2 provided by MODTRAN4 (at 220 K) simultaneously with a linear closure term. The simulated slant column densities do not require any correction for tilt features since MODTRAN4 samples instead of binning.

[25] The onion peel starts at the highest tangent height grid point for which the r^2 of the spectral fit is >0.5 (usually at TH = 40km). The source of the NO_2 profile outside the retrieval range is the MODTRAN4 database from which the appropriate season and latitude band are selected. The number density profile outside the altitude range generally has a small impact on the retrieved profile (see section 2.3) because there is very little NO_2 above 40 km and OSIRIS is fairly insensitive to NO_2 below the tangent height. This is discussed further after the description of the inversion algorithm and in section 2.3. The retrieved profile from the previous scan in the orbit is used as the first guess in the altitude range of the retrieval or, in the absence of this, the scan for the same latitude from the previous orbit is used. The retrieved profile is not sensitive to this first guess; it is used simply to speed up the convergence between model and measurement.

[26] A first guess of the number density ($x_{i=0,z=40}$) begins the iterative retrieval process. The subscripts indicate the iteration number (i) and the altitude (z, in km). This results in a simulated SCD ($y_{0,40}$), which is compared with the measured SCD ($y_{t,40}$). The number density at this altitude is updated ($x_{1,z} = x_{0,z} + \Delta x_{1,z}$) using *Chahine*'s [1970] method

$$x_{1,z} = x_{0,z}\left(y_{t,z}/y_{0,z}\right), \tag{2}$$

i.e.,

$$\Delta x_{1,z} = x_{0,z}\frac{y_{t,z} - y_{0,z}}{y_{0,z}},$$

which ensures that number densities remain positive. This is usually not a good update at low tangent heights where the SCD and number density are not related so simply. However, this iteration provides us with $y_{1,z}$ and then

$$\Delta x_{2,z} = \Delta x_{1,z}\frac{y_{t,z} - y_{1,z}}{|y_{1,z} - y_{0,z}|} \tag{3}$$

usually improves the agreement between model and measurement significantly. In general, the correction $\Delta x_{i+1,z}$ is then, for $i \geq 1$:

$$\Delta x_{i+1,z} = \Delta x_{i,z}\frac{y_{t,z} - y_{i,z}}{|y_{i,z} - y_{i-1,z}|}. \tag{4}$$

In words, the algorithm linearly interpolates or extrapolates the modeled number density based on the preceding two guesses (at most) and consequent local SCD until the modeled SCD approaches the measured SCD. The model and measured SCD profiles are considered to agree when they are within the greater of 3% (i.e., the NO_2 cross section uncertainty [*Vandaele et al.*, 1998]) or the NO_2 SCD fitting uncertainty at each TH, at which point the retrieval terminates. The uncertainty is the 1-σ standard error of the SCD and is provided by the least-squares fitting program. At the NO_2 SCD peak in the scan, the SCD uncertainty is typically 2%. A typical SCD profile with uncertainties is shown below.

[27] To optimize the retrieval algorithm, only the newest (lowest) layer is checked until the SCD at the height of the layer converges with the measured SCD. The impact of adjusting underlying layer densities on the higher THs is not assessed until after the model and measured SCDs have converged at each TH moving sequentially downward. Then the entire SCD profile is modeled to confirm that it has not diverged from the measurement at any altitude. If it has, appropriate layer densities are updated using equations (2) and (4). Five iterations are typically required at each shell.

[28] Two conditional operations are used to either improve the accuracy of the retrieved profile or speed up the convergence between the measurement and the model. In order of implementation, they are as follows: (1) If after update ($\Delta x_{i,z}$), SCD at adjacent TH is more affected than targeted SCD, i.e., $(y_{i,z\pm2} - y_{i-1,z\pm2}) > (y_{i,z} - y_{i-1,z})$, undo update and update other adjacent layer ($\Delta x_{i,z\mp2}$). (2) Regularization: if $x_{i,z} > 2\ x_{i,z\pm1}$, smooth profile using average of two number densities for both layers and then continue (flag and do not re-regularize). However, a doubling in retrieved number density over a 2 km range can occur even with instruments with moderate vertical resolution (see Observations section below). Because the a priori NO_2 profile is, on occasion, quite different from the true profile above the retrieval range, the algorithm does not allow a local maximum or minimum in number density to exist at the upper end of the retrieved profile (i.e., z = 40 km). Instead, the number density in that layer is decreased and the number densities in the immediately overlying layers are increased to yield a profile which increases exponentially with decreasing altitude down to z = 38 km.

[29] With respect to the retrieval of NO_2 from limb scatter, optimal estimation (OE) [*Rodgers*, 1976] is only as robust as the algorithm presented above when the logarithm of both the independent and dependent variable (in this case, SCDs and number densities, respectively) are used in OE. This adaptation of OE is used to recover ozone profiles from OSIRIS [*von Savigny*, 2002]. The algorithm used here reduces computational time because the entire weighting function matrix need not be calculated. OE needs to calculate this matrix at least twice as it iterates toward a solution of comparable accuracy.

2.3. Analysis of Uncertainties and Sensitivities

[30] Number density precision is estimated for each profile by propagating SCD fitting uncertainties through the IOP algorithm. This is achieved by perturbing the tangent layer density until the consequent change in the SCD at that TH exceeds its uncertainty. The magnitude of the perturbation is the random error of the local number density and error bars are assumed symmetrical about the retrieved number density. The precision calculated in this way agrees well with that calculated using OE. Number density uncertainties are a function of the SZA and the NO_2 profile itself but tend to be ~20% at z = 20 and ~30% at z = 40 km and as low as 5% between these two altitudes. At z = 40 km, the uncertainty is dominated by the uncertainty in the first step of the inversion, namely the SCD fitting. At z = 20 km, the uncertainty is dominated by the inability of the inversion algorithm to distinguish small changes in local number density because the bulk of the NO_2 column lies above and because the atmosphere is optically thick with respect to Rayleigh scattering.

[31] The profile uncertainty in the vertical direction is <1.5 km assuming errors in TH translate to equivalent errors in altitude, which is to be expected since the retrieval is insensitive to realistic errors in neutral density as shown below and by *von Savigny* [2002]. There is also an uncertainty in the effective latitude and longitude of the profile due to two effects: (1) spatial sampling and resolution, and (2) near-side dominance in the contribution to the observed radiance. The spatial sampling is dictated by the displacement of the Odin satellite while OSIRIS is limb scanning the stratosphere. This can lead to a longitude range of 6° during stratospheric limb scanning in the worst case scenario at the poles and a latitude range of up to ~5° at the equator. However, the spatial sampling is only ~2° over the retrieval altitude range. The spatial resolution is comparable to the spatial sampling in the along-track direction as the NO_2 absorption signature can come from up to 3° away from the tangent point assuming single scattering only and that the NO_2 lies below z = 40 km. The case which results in the largest spatial range occurs during a down-scan where the spectral image at TH = 40 km is observed ~2° along-track before the spectrum at TH = 18 km. The latter spectrum contains useful information on the NO_2 number density at z = 40 km but from ~1.3° beyond the tangent point of the image at TH = 18 km. Thus, the spatial range in the along-track direction of the NO_2 number density in general is given by the spatial sampling over the retrieval range plus $\frac{1}{2}$ the spatial resolution and amounts to <3.5° in this worst case scenario (z = 40km). The spatial range is smaller for lower altitudes and for up-scans.

[32] We have performed quantitative tests to determine the relative contributions of the near and far side of the limb. The near side of the limb encompasses the atmospheric volume between the observing instrument and plane formed by the radial vector that passes through the tangent point and the vector normal to this and to the line-of-sight (LOS). The far side is the volume lying beyond this plane from the vantage point of the observing instrument. The possible errors introduced by assuming horizontal homogeneity along the LOS were investigated using the radiative transfer model of *McLinden et al.* [2002]. The model has been extended to now include variations of the number density profile of the given constituent along the LOS of the tangent ray. This is achieved by performing many plane-parallel calculations at different SZAs and for different atmospheres. A final LOS integration is then performed over the tangent path using plane-parallel source functions appropriate for that altitude, SZA, and atmosphere. For these tests, SCDs from the 2-D simulation represent the true case and the inversion relies on the 1-D model. The number density profile is scaled by user-defined multiplicative factors 10° away from the tangent point in the LOS direction and linear interpolation is used between the two extreme profiles. In Figure 2, we show the error in the NO_2 profile at the tangent point for a simulated retrieval (neglecting satellite motion) in which a strong gradient exists along the LOS. The magnitude of the near and far side NO_2 profiles have been scaled to 0.5 and 1.5 times the

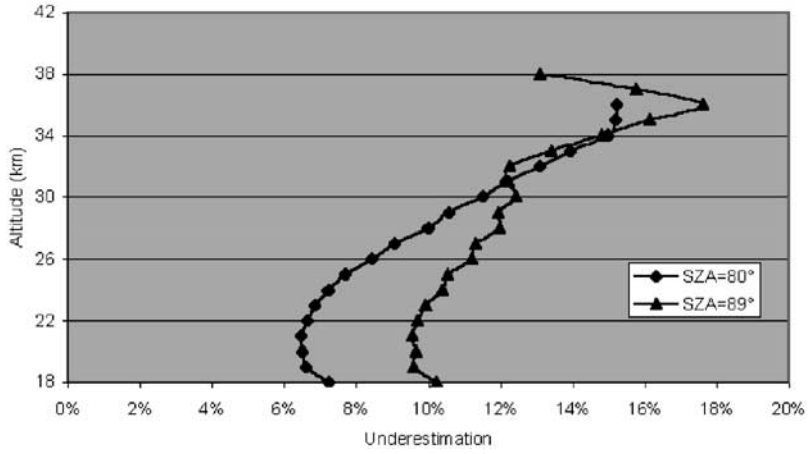

Figure 2. Impact of neglecting near-side dominance to the radiance contribution in the presence of horizontal inhomogeneity in the NO_2 profile along the line-of-sight. Near and far side NO_2 profiles are scaled to 0.5 and 1.5 times the profile at the tangent point and the difference in azimuth angle ($d\phi$) between the instrument and the Sun is 118°.

magnitude at the tangent point, respectively. Alternatively, from these calculations, it is possible to express the error in terms of geo-location. The error is on the order of 0.5° in the LOS direction in a worst-case scenario of high SZA (i.e., 89°). Thus, using the geo-location of the tangent point at a TH in the middle stratosphere (i.e., 30 km), should result in a representative geo-location of the profile.

[33] The sensitivity to the a priori NO_2 profile outside the retrieval range was tested by perturbing the number densities above and below the retrieval range ($z < 19$ km) at SZA = 89° for a profile retrieved below on February 28th, 2002 (see section 3). The a priori contribution, expressed as a percentage and shown in Figure 3, is the absolute magnitude of the % change in the retrieved number density relative to the absolute magnitude of the % perturbation in the a priori profile. For SZA = 57°, the retrieved NO_2 profile only shows a sensitivity to the a priori below the retrieval range. The a priori contribution is 2.3% at $z = 19$ km and decreases monotonically above that. There is no sensitivity to the a priori above the retrieval range (i.e., $z > 39$ km) because the NO_2 signature above this altitude is negligible for this SZA and because the algorithm recognizes that the layers above 39 km need updating and does so with sufficient accuracy. There is also no sensitivity to the first guess in the retrieval range because the method is iterative and several updates are required at each altitude to meet the convergence criteria.

[34] The effect of clouds (or a bright underlying surface) has been investigated and appears to be small in the blue when limb viewing at TH $\geq$ 18 km and SZA > 57°. This conclusion is reached by looking at the assigned weight (or effective path length) below the tangent altitude using the perturbation method of *McDade et al.* [2002] for the calculation. It is 1–2 orders of magnitude smaller than the magnitude (Figure 4) at the tangent height but increases as one looks into the troposphere. This clearly shows one of the benefits of OSIRIS/Odin being in an orbit where the Sun remains low. To quantitatively establish the sensitivity of the stratospheric NO_2 profile on clouds, a retrieval using simulated (noise-free) data was performed for 4 SZAs (30, 57, 79, and 89°) with an optically thick cumulus cloud (top at 3 km, base at 0.66km) used to calculate the 'true' SCD profile but with clouds excluded in the inversion and surface albedo (Λ) of 0.04. A sub-arctic winter NO_2 profile was assumed. Results are shown in Figure 5. The error due to neglecting the presence of clouds in the inversion is systematic and,

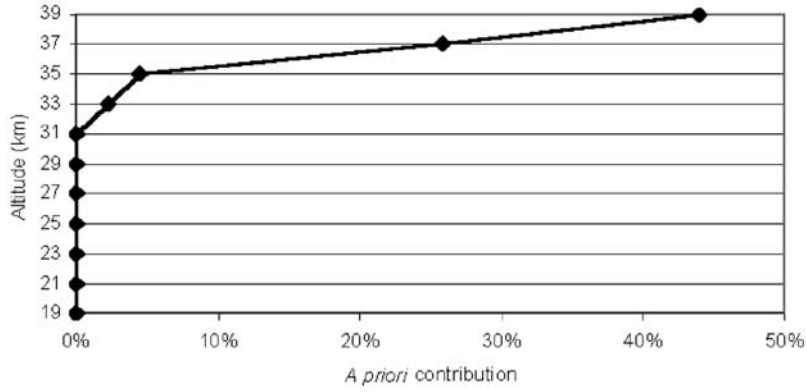

Figure 3. A priori contribution at SZA = 89° (details given in Figure 11d below).

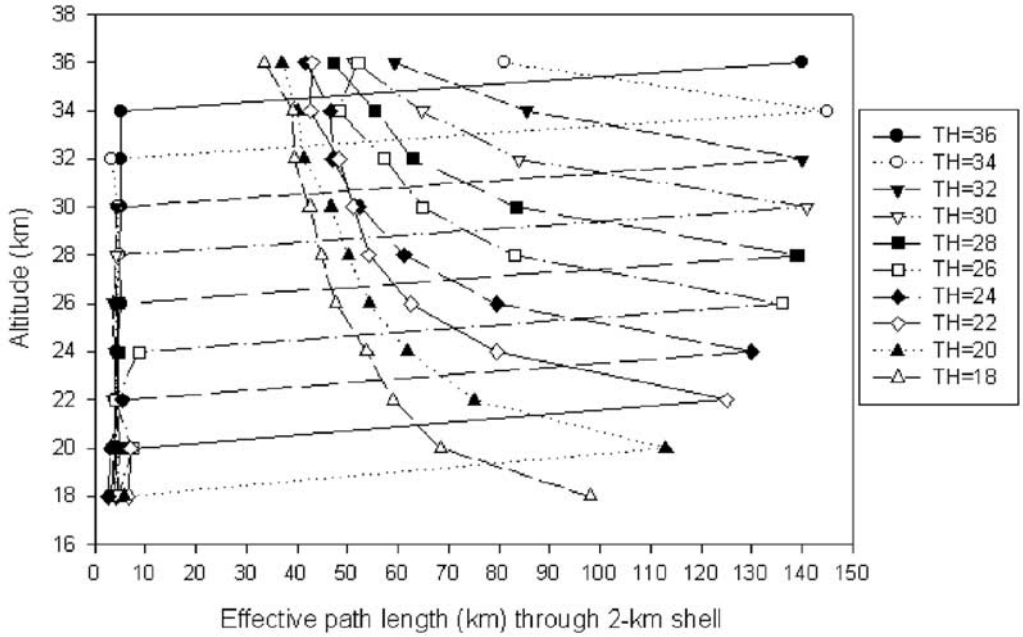

Figure 4. Effective path length for NO_2 absorption in 2-km shell for SZA = 72°, cumulus cloud deck with top and base at 3 and 0.66 km, respectively and extinction of 92.6 km^{-1} (at λ = 550 nm). The effective path length as a function of altitude is the weighting function for a given TH.

strangely, leads to an underestimation of the NO_2 profile. The underestimation cannot be explained by boundary layer NO_2 being screened off by the overlying cloud deck since after removing the boundary layer NO_2 entirely, the underestimation remains practically unchanged. We presume the underestimation is due to the fact that the path enhancement to the high-altitude reference is greater than that for the tangent height of interest. At SZA = 57°, the underestimation of the vertical column density approaches 5% but it is only 2% at 79° and 0% at SZA = 89°. The largest underestimation in local number density tends to occur at either end of the retrieval range. This can be explained as follows: at the upper end of the retrieval range a local maximum occurs because the NO_2 signature in the radiation upwelling through the underlying stratosphere becomes comparable to the single scattering NO_2 signature. At the lower end of the retrieval range, the error tends to be a local maximum because the multiple-scattering contribution is greater than at higher altitudes. Raising the a priori Λ (e.g., Λ = 0.2) can further minimize the sensitivity to clouds since the effects of clouds and bright surfaces should be somewhat interchangeable. Thus, the current assumption of a low surface reflectivity in the inversion maximizes the cloud sensitivity. The sensitivity of the NO_2 profile to high cloud has been tested by introducing a cirrus cloud with top at 10 km and base at 3 km, 64 μm mode radius, and an optical depth of 7. Since high clouds occur mostly in the tropics, we set the SZA to 81° since this is the lowest SZA for the Odin orbit in the

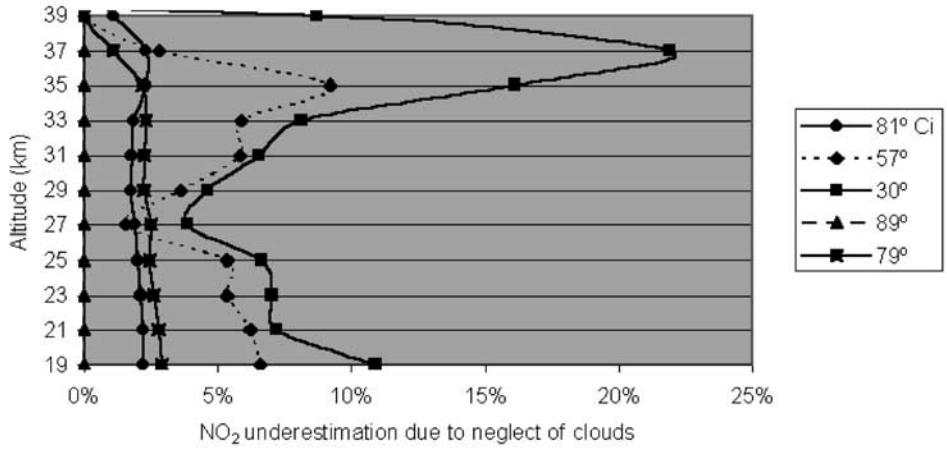

Figure 5. Impact of cloud as a function of SZA (see Figure 4 for details on the cumulus cloud). The cirrus cloud described in the text is labelled 'Ci'.

tropics. Even if cloud tops are as high as 10 km, high cirrus introduces a small, systematic error to the stratospheric NO_2 profile retrieval (Figure 5).

[35] The sensitivity of stratospheric aerosols also appears to be small for OSIRIS. In the retrieval algorithm, the assumed vertical distribution of aerosol optical properties and number densities are obtained from the MODTRAN4 database for the appropriate latitude and season. For SZA = 80°, and a scattering angle of 71°, the error in the retrieved NO_2 profile at all heights when the assumed aerosol profile is changed from background to moderate volcanic is <5% and the NO_2 column error was 0.2%. This aerosol perturbation amounts to more a doubling in the 20–30 km altitude range. However, the largest absolute and relative increase in aerosol number density is at 15 km, and decreases monotonically above this altitude. The largest impact on the NO_2 profile (19–39 km) occurred at 21 km.

[36] There is almost no sensitivity to the assumed pressure profile. This was determined by switching only the pressure profile from mid-latitude summer to mid-latitude winter and verifying that the vertical fitting convergence criterion had been met at all tangent heights using the resulting set of simulated limb radiances. Analogous tests were performed to establish a lack of sensitivity to temperature (mid-latitude summer vs. winter) and to the DISORT 4-stream approximation as to compared to using 8 quadrature points for SZA = 79°, with background aerosols, and $\Lambda = 0.08$. A 2-stream approximation results in very large differences (>10%) in the retrieved NO_2 profile as compared to the 8-stream and is thus inadequate.

[37] Correlation in NO_2 number density between layers is yet another source of error. A partial correlation matrix was established numerically using simulated noise-free data for layers at z = 21, 29, and 37 km, representing layers in the upper, middle and lower portion of the retrieval range. A mid-latitude summer atmosphere was used, with SZA = 72° and $\Lambda = 0.04$. A layer is perturbed by 3e9 molec/cm^3 and then the perturbed profile is retrieved assuming the unperturbed a priori profile. When the 2-km layer whose bottom is at 21 km was perturbed, the retrieved profile agreed with the true (perturbed) profile to better than 2% at all heights, indicating that the other layers are not significantly correlated to the layer at 21 km. The same conclusion was reached upon perturbing the layer at 29 km. The number density at the perturbed layer was retrieved to <0.8% in both cases. Finally, when the layer at 37 km was perturbed, some correlation was observed. This may be partly due to the fact that the perturbation, although constant in absolute magnitude is larger relative to the number density at 37 km than at 29 and 21 km. The 3e9 molec/cm^3 perturbation led to a retrieval error at 35 km of 2.5e8 molec/cm^3. Thus the correlation is the ratio of these values and amounts to 8.5%. The correlation at 39 km is 0.5% and is <0.5% at all other layers. The perturbed layer was underestimated by 4%. The correlation test provides support that the vertical grid size of the retrieval is adequate and that the vertical resolution of the NO_2 profile is clearly $\leq$2 km from 21–29 km, in agreement with *Strong et al.* [2002]. These simulations show the ability of the retrieval algorithm to retrieve sharply peaked profiles.

[38] In summary, only pointing appears to be a significant (>10%) systematic source of error. The magnitude of pointing errors depends directly on the sharpness of the profile. However, errors in the number density profile due to pointing appear to cancel out when vertical column densities are compared (see Validation section below).

[39] Random errors due to instrument noise have been quantified by *McDade et al.* [2002] and *Strong et al.* [2002] and range from 3% at best to 13–20% at 20 km and 30% at 39 km.

3. Observations and Discussion

[40] In this section, the observed differential structure and corresponding spectral fits (Figure 6) are shown along with SCD profiles (Figure 7) and fit residuals (Figures 8a and 8b). Vertical profiles are also presented below. Limb radiance spectra observed by OSIRIS as a function of TH have been illustrated elsewhere [*von Savigny et al.*, 2003].

[41] At the SCD peak, only 2% of the differential optical depth (DOD) is unexplained (Figure 7). The SCD percentage uncertainty increases rapidly above the NO_2 SCD peak and is on the order of 20% at TH = 40 km, but is highly variable because of the sharp gradient in NO_2 at this altitude so uncertainties can range from 10 to 300%. Below the SCD peak, the uncertainties are relatively TH-independent (i.e., 2–3%).

[42] The residuals as a function of TH show a repeating pattern (Figures 8a and 8b), indicating that the fits are not at the shot noise limit. The largest residual occurs at 438 nm, in the wings of Fe I, the largest Fraunhofer lines in the fitting window. The residual appears to increase in magnitude with decreasing TH. This feature and others are likely due to an imperfect 'tilt' correction.

[43] The fitting residuals are not systematically larger at pixels corresponding to Fraunhofer line cores whether the Ring effect correction is performed or not (see Figures 8a and 8b) indicating that in this NO_2 fitting window, the Ring effect cancels out quite well using a high TH reference. This is probably due to a combination of reasons: the fairly low spectral resolution of OSIRIS (1 nm), the fact that the effective temperature of the lower mesospheric reference spectrum is sufficiently close to the temperatures found in the lower and middle stratosphere, and that, during the period of the observations presented here, the stratosphere was extremely clean as can be seen from POAM III aerosol observations www.cpi.com/products/poam/download.html) thus the aerosol dilution effect was small in the blue ($\sim$440 nm). NO_2 SCDs are typically 3% larger when the backward model is applied than if the Ring effect is ignored altogether, presumably due to the removal of weak filling in of NO_2 features as has been discussed for other geometries [e.g., *Vountas et al.*, 1998].

[44] To illustrate the unique spatial and temporal coverage of OSIRIS NO_2 observations, a half-orbit of data was analyzed. We chose Odin's 3446th orbit on Oct 10th when the satellite, moving southward over the Pacific, scanned the limb starting from 40°N (NW USA). The data analysis is limited to SZA < 90°, allowing for coverage into the Antarctic circle (tangent point at 67° S). This orbit was selected for a number of reasons: (1) This is one of two times of the year when OSIRIS is spatially and temporally coincident with the satellite-borne occultation instruments (POAM III and HALOE). This orbit features a HALOE

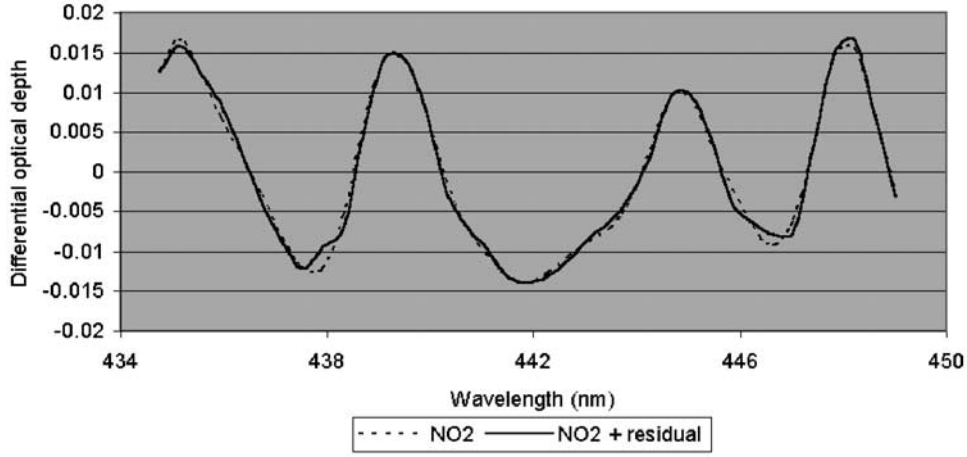

Figure 6. Natural logarithm of the reciprocal of the observed normalized radiance (ln [I_0/I]) on July 30th, 2001, 1 pm UT (lat: 33.5°, lon: 69°), SZA = 75°, TH ≅ 30 km. NO_2 SCD is 6.72e16 molecules/cm^2.

coincidence shown below. (2) Both the southern and northern hemispheres are sunlit on the descending phase of the orbit allowing for coverage from northern mid-latitudes to southern high-latitudes and an investigation of hemispheric asymmetry in NO_2. (3) The SZA is roughly constant during this segment of the orbit (Figure 9) so that the diurnal variation of NO_2 at 30 km is $\leq$10% over the SZA range according to photochemical modeling [*McLinden et al.*, 2001]. The NO_2 is known to vary rapidly between 90 and 92°, but not at SZA < 90°. Thus, this orbit allows latitudinal and diurnal variations to be separated as the entire orbit occurs just after local sunrise, whereas SZAs are much lower at the pole than the equator for Odin at other times of the year. (4) To test the forward RT model (and inversion algorithm) at high SZA.

[45] The Canadian Middle Atmosphere Model (CMAM) [*de Grandpré et al.*, 1997] is used to confirm the altitudinal and latitudinal distribution of NO_2 retrieved by OSIRIS. OSIRIS number densities are interpolated to CMAM pressures using the latitude-dependent pressure profiles assumed in the inversion. Figure 10 shows that the observations are consistent with the CMAM model in most respects, including: (1) In the tropics, the peak is shifted upward and is narrower and the total column is a latitudinal minimum. (2) In the northern hemisphere, the profile is shifted upward relative to the southern hemisphere presumably due to greater tropopause flux in the former. (3) At southern high-latitudes (e.g., 60° S), the NO_2 concentrations in the lower stratosphere are high as the peak shifts downward by 8 km over a narrow latitude range at the edge of the polar vortex.

[46] In contrast to Figure 10b, Figure 10a shows the variability commonly observed in the winter hemisphere at mid-latitudes [*Zawodny*, 1986] where the effect of

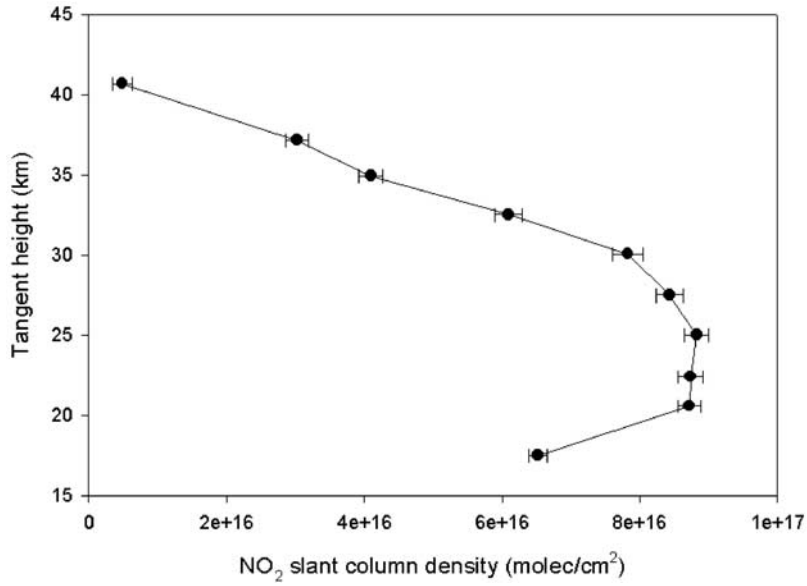

Figure 7. Measured SCD profile (see Figure 6 for details of geo-location).

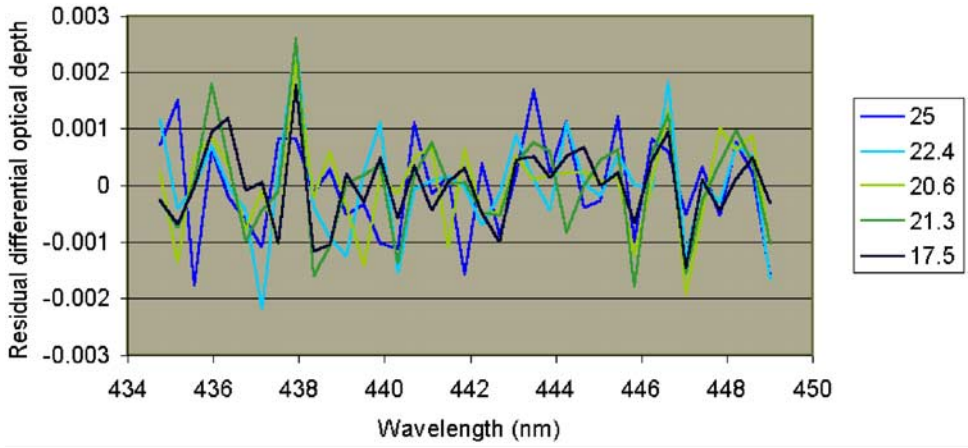

Figure 8a. Fit residuals (435–449 nm) from same scan as in Figure 6. THs (km) are indicated in legend. Ordinate scale shows residual of fit of ln $[I_0/I]$ (see Figure 6).

dynamics is largely responsible for the shape of the profile whereas in equatorial regions, the profile shape is governed by photochemistry.

[47] At the time of the observations, the annual Antarctic ozone hole is well apparent in OSIRIS O_3 profiles. The polar vortex appears to begin at about 63°S for Odin's longitude on this orbit (220°) based on the 220 DU contour on the EarthProbe-TOMS O_3 map for this day. At 67°S, there is ~200 DU of O_3, a far greater vertical column amount than the <100 DU that lies at the pole. Thus, OSIRIS may not have sampled much of the NO_2 depleted air inside the polar vortex on this orbit.

[48] OSIRIS NO_2 profiles are compared with correlative measurements by a variety of validated NO_2 profiling instruments such as HALOE [*Gordley et al.*, 1996], POAM III [e.g., *Randall et al.*, 2002], and LPMA/DOAS [*Ferlemann et al.*, 2000] as a function of season (summer and winter), latitude (high, low, and mid-latitude) and time of day (sunrise, midday, sunset). Coincidence criteria, following *Randall et al.* [2002] are ±4° in latitude, ±12° longitude, and ±2 hours in time. An additional criterion is included: the SZA of the coincident measurements must be comparable so that the NO_2 profile at that time and place does not change by >15% according to photochemical modeling [*McLinden et al.*, 2001]. Retrieved profiles from the instrument with superior vertical resolution are not convolved to match the vertical resolution of the other coincident instrument.

[49] The flight of LPMA/DOAS (Laboratoire Physique Moléculaire et Applications/Differential Optical Absorption Spectroscopy) balloon payload at Kiruna (67.9°N, 21.2°E) on August 21–22, 2001 allowed for the validation of the coincident daytime NO_2 profile observed by OSIRIS. The azimuth-controlled LPMA/DOAS payload carries two UV/vis balloon-borne spectrometers and a FT-IR instrument that measured NO_2 profiles in direct sun during balloon ascent (SZA = 77° to 88°). The profile measured by the visible DOAS instrument (420–465 nm) during the ascent phase of the LPMA/DOAS balloon flight (Figure 11) is typically within 15% of OSIRIS and the vertical columns are within 14% with very good agreement on the peak altitude (~25 km) during this northern high-latitude afternoon coincidence in late summer. The difference in the profile between 25–30 km may be explained by noting that the ascent profile takes place after the OS limb scan and that

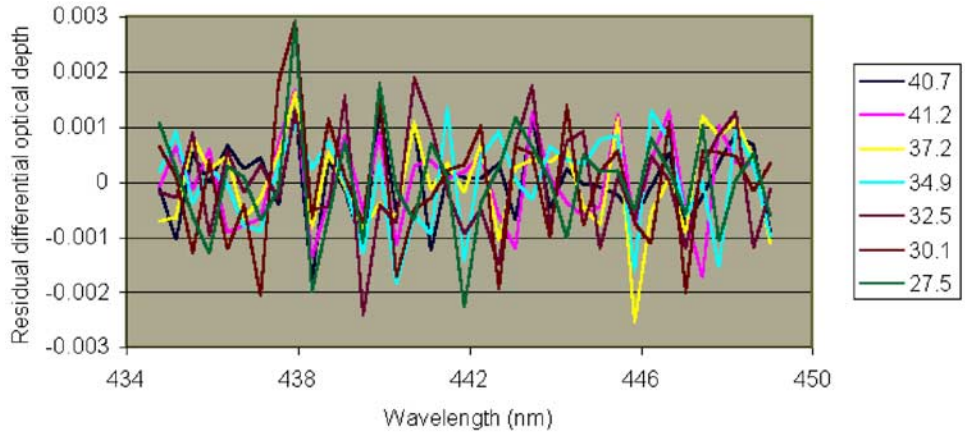

Figure 8b. Same as Figure 8a, except for higher THs. At TH ≅ 40 km, the rms residual is typically on the order of 6e-4.

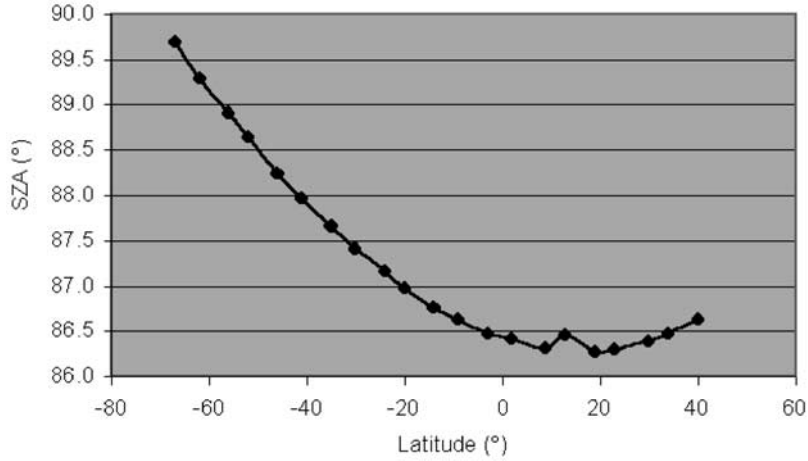

Figure 9. SZA (at tangent point for TH = 30 km) vs. latitude during orbit 0D76 on October 10th, 2001.

N_2O_5 dissociation, primarily by photolysis [*McLinden et al.*, 2002], continues throughout the day mostly at these altitudes. After correcting for the diurnal variation through the use of a photochemical model [*McLinden et al.*, 2002], OSIRIS and LPMA/DOAS agree to 10% on the vertical profile and 6% on the vertical column.

[50] In general, agreement with HALOE (Figures 12a–12d) is 18% on profiles in the 19–39 km range and the agreement on the stratospheric column is excellent (2%) as pointing errors appear to cancel out when integrated vertically. HALOE finds a slightly higher column abundance in cases shown in Figures 12a–12b and 12d, which is consistent with the fact that the NO_2 abundance should increase slightly with SZA from ~87° to 90° (see captions of Figures 12a, 12b, and 12d). The profile that includes photochemical forward modeling in Figure 12c was used in the aforementioned column and profile statistics for the three correlative HALOE measurements. OSIRIS and HALOE columns at SZA = 90° in Figure 12c agree to 1%. The agreement with HALOE in Figure 12d demonstrates that the assumption of horizontal homogeneity in the vicinity of the tangent point in the along-track direction appears to be adequate even though a large diurnal NO_2 gradient is expected beyond the terminator Furthermore, at high SZA (e. g. 89.5°, $d\phi$ = 93°, TH = 30 km, Λ = 0.04 and 440.5 nm), single scattering accounts for 98.5% of the total radiance. The measured radiance therefore contains the NO_2 signature of the sunlit atmosphere and thus does not contain significant signature from multiple scattering in the twilit NO_2-rich side of the terminator. Also, OSIRIS does not look normal to the terminator instead it roughly looks along it (±33°), minimizing the expected diurnal gradient.

[51] The comparison with POAM III again showed the ability of OSIRIS to accurately measure the shape and peak altitude of a given NO_2 profile as the coincident satellite observations agree to 14% on average between 21 and 37 km. Since the SZA approached 90° and atmospheric sphericity becomes increasingly important, the variation in SZA during the scan is taken into account (to 3 significant digits)

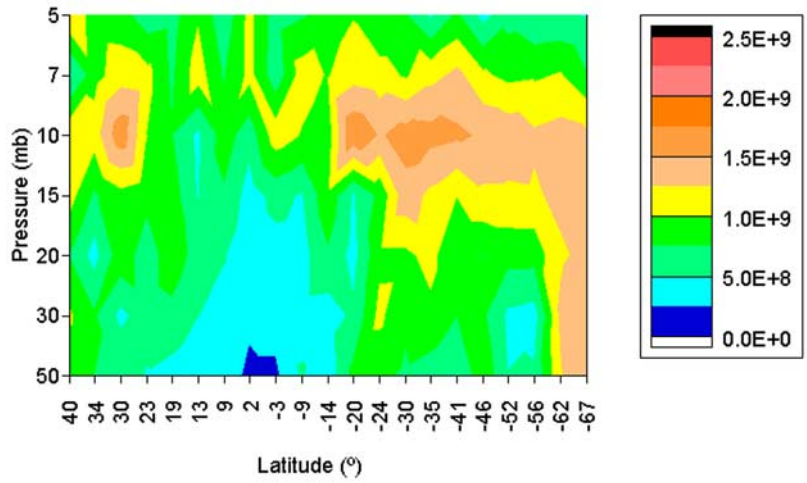

Figure 10a. Snapshot of latitudinal distribution of NO_2 number density (cm^{-3}) on Oct 10th (14:30 to 15 pm UT), At lat = 40°, lon = 254° and at lat = −67°, lon = 220°.

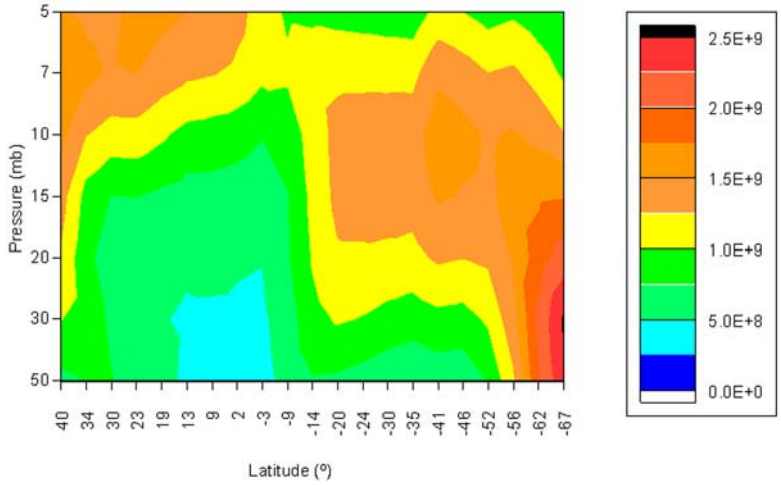

Figure 10b. CMAM contour plot of NO_2 number density (cm^{-3}) over same latitude range and solar conditions: October average.

in the OSIRIS inversion algorithm. The peak altitude is lower than in Figure 11 which shows a similar latitude band ~2 months earlier (August). This seasonal variation in peak height is consistent with CMAM.

[52] These comparisons with solar-occulting instruments show the ability of the retrieval algorithm (including MODTRAN4, its forward RTM) to accurately invert slant column densities in these difficult cases. Thus, it appears thus far that OSIRIS will be an excellent choice to validate future NO_2 profiling instruments, such as recently launched SAGE III [*McCormick et al.*, 1991] and SCIAMACHY.

4. Conclusions and Future Work

[53] A new pseudo-absorber is found which should be important for a variety of viewing geometries and fitting windows. This spectral artefact results from a combination

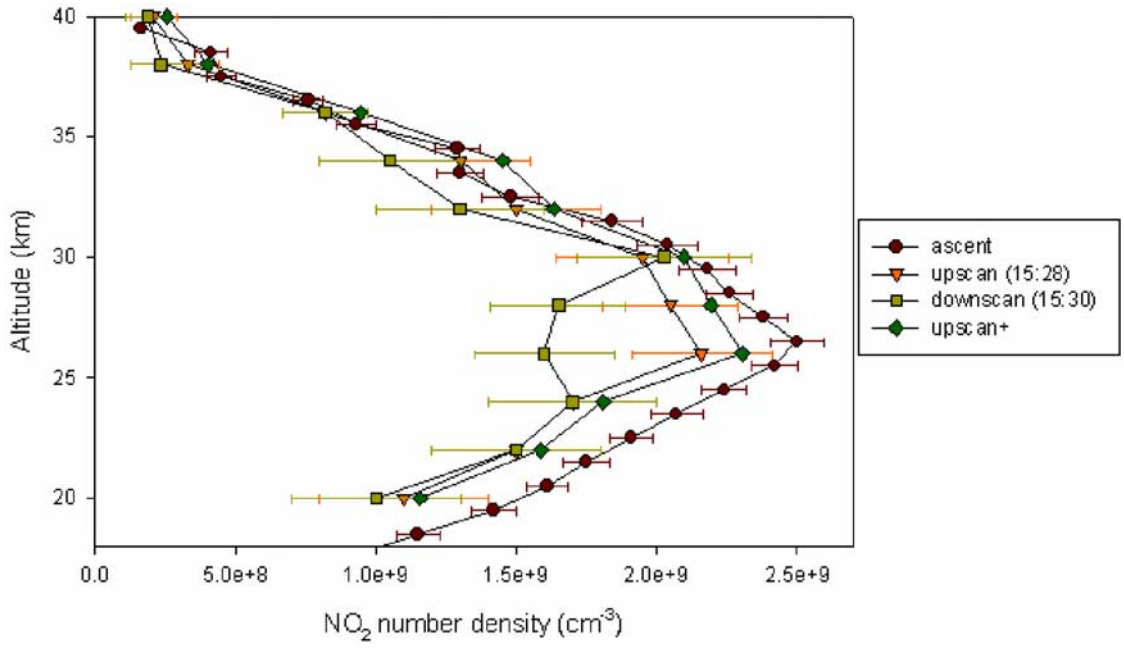

Figure 11. 'Upscan' and 'downscan' are consecutive OSIRIS limb scans southeast (lat = 64°, lon = 23°, SZA = 72°) and northwest (lat = 70°, lon = 16°, SZA = 71°) respectively of balloon ascent location (lat = 68°, lon = 21.2°). Odin was scanning above the stratosphere as it passed over the ascent location. 'Upscan+' contains forward modeling of the diurnal variation of NO_2 due to photochemistry from OSIRIS local time to LPMA/DOAS local time. Error bars are omitted for clarity on the latter profile.

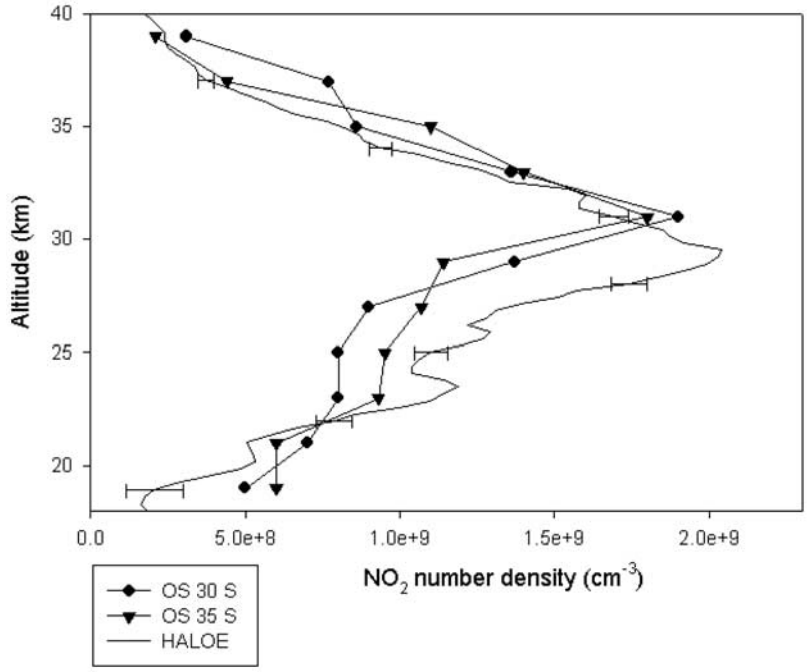

Figure 12a. Spot comparison of NO_2 observed during OSIRIS/HALOE spatial and temporal coincidence at sunrise on Oct 10th, 2001 (contains two successive OSIRIS profiles from Figure 10a). OSIRIS tangent point at TH = 30 km and lat = −30.4°: SZA = 87.4°, lon = 237.4° and time = 13:51 UT; OSIRIS tangent point at TH = 30 km and lat = −35°: SZA = 87.7°, lon = 236°, and time = 13:52 UT; HALOE coordinates are lat = −32.7°, lon = 248.7°, time = 12:54 UT, and SZA = 90°. OSIRIS error bars are omitted for clarity.

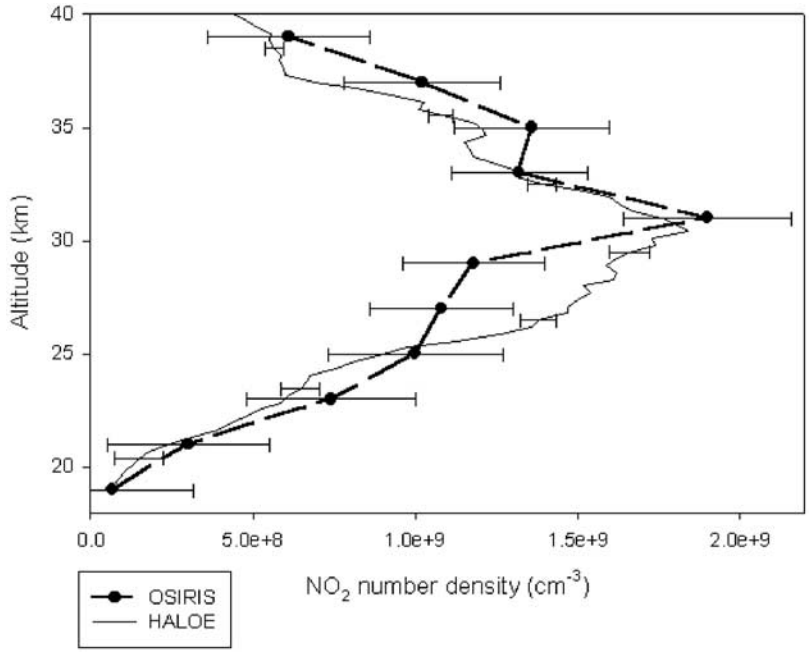

Figure 12b. Comparison of tropical NO_2 profile with HALOE during a sunset coincidence on Feb. 15th, 2002. OSIRIS lat = −1.9°, SZA = 86.63°, lon = 62.3° and time = 13:50 UT; HALOE coordinates were lat = −2.64°, lon = 68.87°, time = 13:40 UT, and SZA = 90°. HALOE also has a vertical resolution of ∼2 km [*Gordley et al.*, 1996].

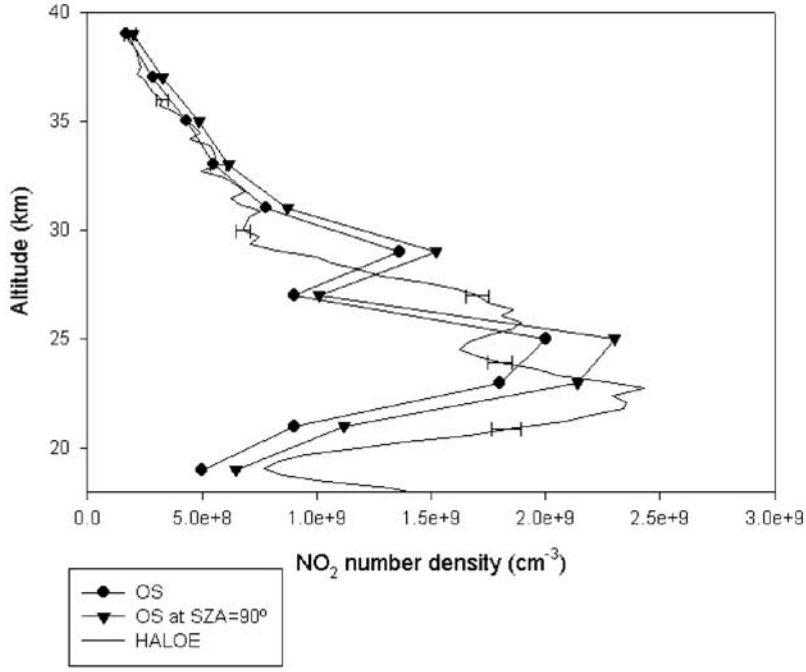

Figure 12c. Comparison of NO_2 profile in Antarctic ozone hole conditions with HALOE during a sunrise ''coincidence'' on Oct. 24th, 2001. OSIRIS lat = −67.7°, lon = 3.4°, SZA = 85.2°, and time = 4:25 UT; HALOE coordinates are lat = −69.0°, lon = 5.1°, time = 3:13 UT, and SZA = 90°. Yellow triangles include altitude-dependent forward modeling of OSIRIS profile from SZA = 85° to 90° based on photochemical calculations (without heterogeneous chemistry) for October a.m. at 80° S [*McLinden et al.*, 2001]. Error bars are omitted for clarity.

of spectral undersampling and convolution, Fraunhofer structure, and Rayleigh extinction and cannot be removed by a polynomial. Also with regard to the spectral fitting, the spectral resolution of OSIRIS in this fitting window needs to be pinpointed to reduce uncertainties in the retrieved profiles.

[54] The inclusion of multiple scattering has allowed NO_2 profiles retrieved from OSIRIS limb spectra to extend

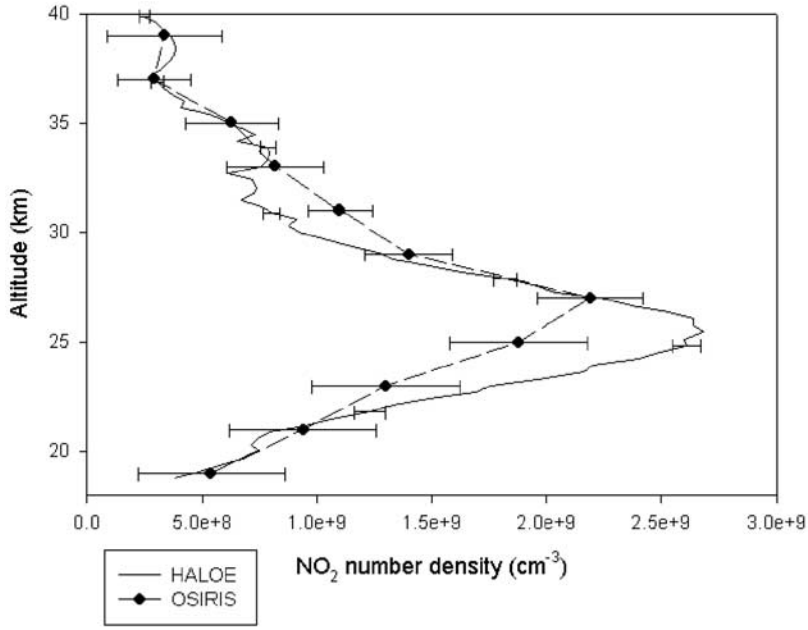

Figure 12d. Mid-latitude winter (28.02.2002) sunset coincidence between HALOE and OSIRIS (lat = 59.7°).

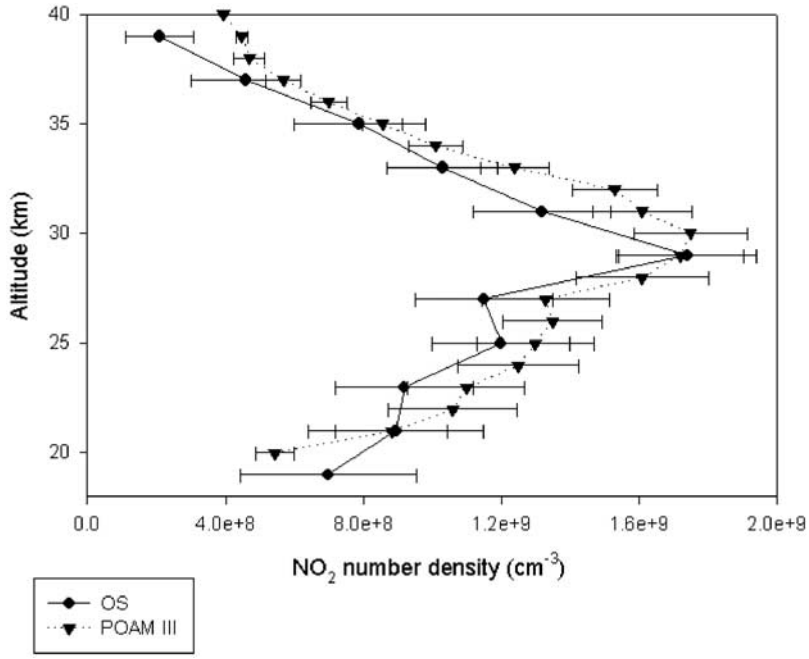

Figure 13. Spot comparison of NO2 observed during OSIRIS/POAM III spatial and temporal coincidence at sunset on Oct 10th, 2001. OSIRIS SZA (at tangent point) varies in the range 89.947–89.868° for 18 < TH(km) < 41.09, with lat = 74°, lon = 353° and time = 16:28 UT at TH = 30 km. POAM III coordinates are lat = 71°, lon = 2°, time = 16:17 UT, and SZA = 90°.

into the lower stratosphere (i.e., 17.5 km for low SZA) whereas previous work with the SME was limited to a lower altitude of 26 ± 2 km [*Thomas et al.*, 1988; *Mount et al.*, 1984] because of the single scattering approximation in the forward RTM. Non-linearity, caused by primarily by Rayleigh scattering, necessitates an iterative retrieval algorithm. A single iteration of optimal estimation [*Rodgers*, 1976] or a simple onion peel using the same weighting function matrix generated with an a priori profile has been tried and is not sufficient. Studies have been performed to quantify the sensitivity to a priori NO_2, stratospheric aerosols, pressure, and temperature and clouds. The validity of the 4-stream approximation has been confirmed. Other systematic sources of error that have been considered include pointing, baffle scattering, polarization, internal scattering, wavelength drift. The retrieval is sensitive near the retrieval altitude limits to the a priori NO_2 information from outside the retrieval range. In conclusion, shot noise is comparable to the systematic sources of error in the inversion algorithm.

[55] The novel algorithm presented above is stable and consistently returns profiles that are in good agreement with correlative measurements. These include spot comparisons with POAM III for northern high-latitude winter (Figure 13), with LPMA/DOAS for northern high-latitude summer (Figure 11), with HALOE for southern high and mid-latitude summer, northern mid-latitude winter and in the tropics (Figures 12c, 12a, 12d, and 12b, respectively). As mentioned in the introduction, the southern hemisphere cannot be viewed in austral winter. Where necessary, comparisons include photochemical forward modeling to the SZA of the correlative data.

[56] In summary, OSIRIS appears to measure stratospheric NO_2 columns with a 1-σ accuracy of 6% (typically) and profiles to <20% at all times of day and all seasons and latitudes in the 20–39 km range. Preliminary statistical analysis of the validated profiles indicates that OSIRIS does not show a systematic bias in any part of the retrieval range. These comparisons with instruments capable of equal or greater vertical resolution have also shown that OSIRIS can partially resolve some small-scale NO_2 structures.

[57] Based on the results presented here, OSIRIS will be invaluable in the early validation of NO_2 profiles from the recently launched SCIAMACHY and SAGE III satellite instruments. Moreover, OSIRIS provides stratospheric NO_2 monitoring with an unprecedented combination of accuracy, spatial coverage and resolution (vertically and latitudinally), and temporal coverage. Together with subsequent instruments, OSIRIS will give a more complete picture of trends in NO_2 and NO_y.

[58] **Acknowledgments.** Odin is a Swedish-led satellite project funded jointly by the Swedish National Space Board (SNSB), the Canadian Space Agency (CSA), the National Technology Agency of Finland (Tekes) and Centre National d'Etudes Spatiales (CNES). The Swedish Space Corporation has been the industrial prime contractor. This work was also supported by the National Sciences and Engineering Research Council (Canada). We are extremely grateful to the entire Odin team. We are indebted to the POAM III, HALOE and Earth Probe-TOMS teams for making their data readily available.

References

Berk, A., G. P. Anderson, P. K. Acharya, J. H. Chetwynd, L. S. Bernstein, E. P. Shettle, M. W. Matthew, and S. M. Adler-Golden, MODTRAN4 User's manual: Software manual, Air Force Res. Lab., Space Vehicles Dir., Air Force Mater. Command, Hanscom Air Force Base, Mass., 1999.

Bogumil, K., J. Orphal, S. Voigt, H. Bovensmann, O. C. Fleischmann, M. Hartmann, T. Homann, P. Spietz, A. Vogel, and J. P. Burrows, Reference spectra of atmospheric trace gases measured the SCIAMACHY PFM satellite spectrometer, paper presented at European Symposium on Atmospheric Measurements From Space, Eur. Space Res. and Technol. Cent., Noordwijk, Netherlands, 1999.

Bovensmann, H., J. P. Burrows, M. Buchwitz, J. Frerick, S. Noël, V. V. Rozanov, K. V. Chance, and A. P. H. Goede, SCIAMACHY: Mission objectives and measurement modes, *J. Atmos. Sci.*, *56*, 127–150, 1999.

Burrows, J. P., A. Richter, A. Dehn, B. Deters, S. Himmelmann, S. Voigt, and J. Orphal, Atmospheric remote sensing reference data from GOME, 2, Temperature dependent absorption cross sections of O_3 in the 234–794 nm range, *J. Quant. Spectrosc. Radiat. Transfer*, *61*, 509–517, 1999a.

Burrows, J. P., et al., The Global Ozone Monitoring Experiment (GOME): Mission concept and first scientific results, *J. Atmos. Sci.*, *56*, 151–175, 1999b.

Camy-Peyret, C., J.-M. Flaud, J.-Y. Mandin, J.-P. Chevillard, J. Brault, D. A. Ramsay, M. Vervloet, and J. Chauville, The high-resolution spectrum of water vapor between 16500 and 25250 cm^{-1}, *J. Mol. Spectrosc.*, *113*, 208–228, 1985.

Carlotti, M., Global-fit approach to the analysis of limb-scanning atmospheric measurements, *Appl. Opt.*, *27*, 3250–3254, 1988.

Chahine, M. T., Inverse problems in radiative transfer: Determination of atmospheric parameters, *J. Atmos. Sci.*, *27*, 960–967, 1970.

Chance, K., Analysis of BrO measurements from the Global Ozone Monitoring Experiment, *Geophys. Res. Lett.*, *25*, 3335–3338, 1998.

Crutzen, P. J., The influence of nitrogen oxides on the atmospheric ozone content, *Q. J. R. Meterol. Soc.*, *96*, 320–325, 1970.

Crutzen, P. J., Ozone production rates in an oxygen-hydrogen-nitrogen oxide atmosphere, *J. Geophys. Res.*, *76*, 7311–7327, 1971.

Cunnold, D. M., et al., Validation of SAGE II NO_2 measurements, *J. Geophys. Res.*, *96*, 12,913–12,925, 1991.

de Grandpré, J., J. W. Sandilands, J. C. McConnell, S. R. Beagley, P. C. Croteau, and M. Y. Danilin, Canadian Middle Atmosphere Model: Preliminary results from the chemical transport module, *Atmos. Ocean*, *35*, 385–431, 1997.

Evans, W. F. J., and J. M. Alfred, Algorithm for correction of internal scattering and spectral cross-talk in the UV/vis band of the OSIRIS instrument flight model, OSIRIS internal report, Trent Univ., Peterborough, Ont., Canada, 2001.

Ferlemann, F., N. Bauer, R. Fitzenberger, H. Harder, H. Osterkamp, D. Perner, U. Platt, M. Schneider, P. Vradelis, and K. Pfeilsticker, Differential optical absorption spectroscopy instrument for stratospheric balloon trace-gas studies, *Appl. Opt.*, *39*, 2377–2386, 2000.

Flittner, D. E., P. K. Bhartia, and B. M. Herman, O_3 profiles retrieved from limb scatter measurements: Theory, *Geophys. Res. Lett.*, *27*, 2601–2604, 2000.

Garcia, R. R., and S. Solomon, A new numerical model of the middle atmosphere, 2, Ozone and related species, *J. Geophys. Res.*, *99*, 12,937–12,951, 1994.

Gordley, L. L., et al., Validation of nitric oxide and nitrogen dioxide measurements made by the Halogen Occultation Experiment for UARS platform, *J. Geophys. Res.*, *101*, 10,241–10,266, 1996.

Grainger, J. R., and J. Ring, Anomalous Fraunhofer line profiles, *Nature*, *193*, 7621962.

Greenblatt, G. D., J. J. Orlando, J. B. Burkholder, and A. R. Ravishankara, Absorption measurements of oxygen between 330 and 1140 nm, *J. Geophys. Res.*, *95*, 18,577–18,582, 1990.

Hedin, A. E., Extension of the MSIS Thermospheric Model into the middle and lower atmosphere, *J. Geophys. Res.*, *96*, 1159–1172, 1991.

Hilsenrath, E., Rocket observations of the vertical distribution of ozone in the polar night and during a mid-winter stratospheric warming, *Geophys. Res. Lett.*, *7*, 581–584, 1980.

Johnston, P. V., and R. L. MacKenzie, NO_2 observations at 45°S during the decreasing phase of solar cycle 21, from 1980 to 1987, *J. Geophys. Res.*, *94*, 3473–3486, 1989.

Joiner, J., P. K. Bhartia, R. P. Cebula, E. Hilsenrath, R. D. McPeters, and H. Park, Rotational Raman scattering (Ring effect) in satellite ultraviolet measurements, *Appl. Opt.*, 4513–4525, 1995.

Llewellyn, E. J., et al., OSIRIS-an application of tomography for absorbed emissions in remote sensing, in *Applications of Photonic Technology*, edited by G. A. Lampropoulos and R. A. Lessard, pp. 627–632, Plenum, New York, 1997.

Lucke, R. L., et al., The Polar Ozone and Aerosol Measurement (POAM) II instrument and early validation results, *J. Geophys. Res.*, *104*, 18,785–18,799, 1999.

McCormick, M. P., W. P. Chu, J. M. Zawodny, L. E. Mauldin, and L. R. McMaster, Stratospheric Aerosol and Gas Experiment III (SAGE III) aerosol and trace gas measurements for Earth Observing System (EOS), *Proc. SPIE Int. Soc. Opt. Eng.*, *1491*, 125–141, 1991.

McDade, I. C., K. Strong, C. S. Haley, J. Stegman, D. P. Murtagh, and E. J. Llewellyn, A method for recovering stratospheric minor species densities from the ODIN/OSIRIS scattered sunlight measurements, *Can. J. Phys.*, *80*, 395–408, 2002.

McElroy, C. T., Stratospheric nitrogen dioxide concentrations as determined from limb brightness measurements made on June 17th, 1983, *J. Geophys. Res.*, *93*, 7075–7083, 1988.

McLinden, C. A., S. C. Olsen, M. J. Prather, and J. B. Liley, Understanding trends in stratospheric NO_y and NO_2, *J. Geophys. Res.*, *106*, 27,787–27,793, 2001.

McLinden, C. A., J. C. McConnell, K. Strong, I. C. McDade, R. L. Gattinger, R. King, B. Solheim, and E. J. Llewellyn, The impact of the OSIRIS grating efficiency on total radiance and trace-gas retrievals, *Can. J. Phys.*, *80*, 469–481, 2002.

McPeters, R. D., S. J. Janz, E. Hilsenrath, T. L. Brown, D. E. Flittner, and D. F. Heath, The retrieval of O_3 profiles from limb scatter measurements: Results from the Shuttle Ozone Limb Sounding Experiment, *Geophys. Res. Lett.*, *27*, 2597–2600, 2000.

Moore, C. E., M. G. J. Minnaert, and J. Houtgast, The solar spectrum: 2935 Å to 8770 Å: Second revision to Rowland's preliminary table of solar spectrum wavelengths, *Monogr. 61*, Natl. Bur. of Stand., U.S. Dep. of Comm., Washington, D. C., 1966.

Mount, G. H., D. W. Rusch, J. F. Noxon, J. M. Zawodny, and C. A. Barth, Measurements of stratospheric NO_2 from the Solar Mesosphere Explorer Satellite, 1, An overview of the results, *J. Geophys. Res.*, *89*, 1327–1340, 1984.

Murtagh, D., et al., An overview of the Odin atmospheric mission, *Can. J. Phys.*, *80*, 309–318, 2002.

Noxon, J. F., Nitrogen dioxide in the stratosphere and troposphere measured by ground-based absorption spectroscopy, *Science*, *189*, 547–549, 1975.

Pfeilsticker, K., H. Bösch, C. Camy-Peyret, R. Fitzenberger, H. Harder, and H. Osterkamp, First atmospheric measurements of UV/visible absorption intensities: Implications for the spectroscopy, and formation enthalpy of the O_2-O_2 dimer, *J. Geophys. Res.*, *28*, 4595–4598, 2001.

Platt, U., L. Marquard, T. Wagner, and D. Perner, Corrections for zenith scattered light DOAS, *Geophys. Res. Lett.*, *24*, 1759–1762, 1997.

Randall, C. E., et al., Validation of POAM III NO_2 measurements, *J. Geophys. Res.*, *107*(D20), 4432, doi:10.1029/2001JD001520, 2002.

Rodgers, C. D., Retrieval of atmospheric temperature and composition from remote measurements of thermal radiation, *Rev. Geophys.*, *14*, 609–624, 1976.

Roscoe, H. K., D. J. Fish, and R. L. Jones, Interpolation errors in UV-visible spectroscopy for stratospheric sensing: implications for sensitivity, spectral resolution, and spectral range, *Appl. Opt.*, *35*, 427–432, 1996.

Sioris, C. E., The filling in of absorption lines in sky spectra due to rotational Raman scattering, Ph. D. thesis, 135 pp., York Univ., Toronto, May 2001.

Sioris, C. E., W. F. J. Evans, R. L. Gattinger, I. C. McDade, D. A. Degenstein, and E. J. Llewellyn, Ground-based Ring effect measurements with the OSIRIS DM, *Can. J. Phys.*, *80*, 483–491, 2002.

Strong, K., B. M. Joseph, R. Dosanjh, I. C. McDade, C. A. McLinden, J. C. McConnell, J. Stegman, D. P. Murtagh, and E. J. Llewellyn, Retrieval of concentration profiles from OSIRIS UV-visible limb spectra, *Can. J. Phys.*, *80*, 409–434, 2002.

Thomas, R. J., K. H. Rosenlof, R. T. Clancy, and J. Zawodny, Stratospheric NO_2 over Antarctica as measured by the Solar Mesosphere Explorer during austral spring, 1986, *J. Geophys. Res.*, *93*, 12561–12568, 1988.

Vandaele, A. C., C. Hermans, P. C. Simon, M. Carleer, R. Colin, S. Fally, M. F. Mérienne, A. Jenouvrier, and B. Coquart, Measurements of NO_2 absorption cross-section from 42000 cm^{-1} to 10000 cm^{-1} (238–1000 nm) at 220 K and 298 K, *J. Quant. Spectrosc. Radiat. Transfer*, *59*, 171–184, 1998.

von Savigny, C., Retrieval of stratospheric ozone density profiles from OSIRIS scattered sunlight observations, Ph.D. thesis, 156 pp., York Univ., Toronto, April 2002.

von Savigny, C., et al., Stratospheric ozone profiles retrieved from limb scattered sunlight radiance spectra measured by the OSIRIS instrument on the Odin satellite, *Geophys. Res. Lett.*, *30*, doi:10.1029/2002GL016401, in press, 2003.

Vountas, M., V. V. Rozanov, and J. P. Burrows, Ring effect: Impact of rotational Raman scattering on radiative transfer in Earth's atmosphere, *J. Quant. Spectrosc. Radiat. Transfer*, *60*, 943–961, 1998.

Warshaw, G. D., D.-L. Desaulniers, and D. Degenstein, Optical design and performance of the performance of the ODIN UV/visible spectrograph and infrared imager system, paper presented at Technical Session XII, paper presented at 10th Annual AIAA/Utah State University Conference on Small Satellites, Am. Inst. of Aeronaut. and Astronaut., Logan, Utah, 1996.

Zawodny, J. M., Short-term variability of nitrogen dioxide in the winter stratosphere, *J. Geophys. Res.*, *91*, 5439–5450, 1986.

Zobov, N. F., et al., The near-ultraviolet rotation-vibration spectrum of water, *J. Chem. Phys.*, *113*, 1546–1552, 2000.

H. Bösch, K. Pfeilsticker, and F. Weidner, Institute of Environmental Physics, University of Heidelberg, INF 229, D-69120 Heidelberg, Germany. (pf@iup.uni-heidelberg.de)

K. Chance, T. P. Kurosu, and C. E. Sioris, Atomic and Molecular Physics Division, Harvard-Smithsonian Center for Astrophysics, Cambridge, MA 02138, USA. (kchance@cfa.harvard.edu; tkurosu@cfa.harvard.edu; csioris@cfa.harvard.edu)

W. F. J. Evans, Department of Physics, Trent University, Peterborough, Canada K9J 7B8. (wevans@trentu.ca)

U. Frisk, Swedish Space Corporation, P. O. Box 4207, Solna SE-171 04, Sweden.

C. S. Haley, J. C. McConnell, and I. C. McDade, Centre for Research in Earth and Space Science, York University, 113 Petrie Building, 4700 Keele Street, Toronto, Ontario, Canada M3J 1P3. (jack@nimbus.yorku.ca; mcdade@yorku.ca)

E. J. Llewellyn and N. D. Lloyd, Department of Physics and Engineering Physics, University of Saskatchewan, 116 Science Place, Saskatoon, Saskatchewan, Canada S7N 5E2. (llewellyn@skisas.usask.ca)

C. A. McLinden, Air Quality Research Branch, Meteorological Service of Canada, 4905 Dufferin Street, Toronto, Ontario, Canada M3H 5T4. (chris.mclinden@ec.gc.ca)

G. Mégie, Service d'Aeronomie du CNRS, IPSL-Université Pierre et Marie Curie, F-75252 Paris Cedex 05, France.

D. Murtagh, Department of Radio and Space Science, Chalmers University, Göteberg SE-41296, Sweden. (donal@rss.chalmers.se)

J. Stegman, Department of Meteorology, Stockholm University, Stockholm SE-106 91, Sweden. (jacek@misu.su.se)

K. Strong, Department of Physics, University of Toronto, Room MP 710A, 60 St. George Street, Toronto, Ontario, Canada M5S 1A7. (strong@atmosp.physics.utoronto.ca)

C. von Savigny, Institute of Environmental Physics, University of Bremen, NW1, Otto-Hahn-Allee 1, Bremen D-28359, Germany. (csavigny@iup.physik.uni-bremen.de)